Available online at www.sciencedirect.com
ScienceDirect
Mechanical Systems and Signal Processing 21 (2007) 706–723
Mechanical Systems and Signal Processing
www.elsevier.com/locate/jnlabr/ymssp

Multi-rate Kalman filtering for the data fusion of displacement and acceleration response measurements in dynamic system monitoring

Andrew Smyth*, Meiliang Wu

Department of Civil Engineering and Engineering Mechanics, Columbia University, New York, NY 10027, USA

Received 19 September 2005; received in revised form 11 January 2006; accepted 11 March 2006
Available online 19 May 2006

Abstract

Many damage detection and system identification approaches benefit from the availability of both acceleration and displacement measurements. This is particularly true in the case of suspected non-linear behavior and permanent deformations. In civil and mechanical structural modeling accelerometers are most often used, however displacement sensors, such as non-contact optical techniques as well as GPS-based methods for civil structures are becoming more common. It is suggested, where possible, to exploit the inherent redundancy in the sensor information and combine the collocated acceleration and displacement measurements in a manner which yields highly accurate motion data. This circumvents problematic integration of accelerometer data that causes low-frequency noise amplification, and potentially more problematic differentiation of displacement measurements which amplify high-frequency noise. Another common feature of displacement-based sensing is that the high-frequency resolution is limited, and often relatively low sampling rates are used. In contrast, accelerometers are often more accurate for higher frequencies and higher sampling rates are often available. The fusion of these two data types must, therefore, combine data sampled at different frequencies. A multi-rate Kalman filtering approach is proposed to solve this problem. In addition, a smoothing step is introduced to obtain improved accuracy in the displacement estimate when it is sampled at lower rates than the corresponding acceleration measurement. Through trials with simulated data the procedure's effectiveness is shown to be quite robust at a variety of noise levels and relative sample rates for this practical problem.

Keywords: Kalman filter; Smoothing; Multi-rate sampling; System identification

1. Introduction

In the past two decades, structural health monitoring (SHM) using vibration measurements has attracted considerable attention in the aerospace, mechanical, and civil engineering communities. In order to conduct on-line monitoring and system identification of structural parameters, the availability of acceleration response measurements as well as displacement response data is often required. Displacement, or deformation,

*Corresponding author. Tel.: +1 2128543369; fax: +1 2128546267.
E-mail address: smyth@civil.columbia.edu (A. Smyth).

0888-3270/$ - see front matter © 2006 Elsevier Ltd. All rights reserved.
doi:10.1016/j.ymssp.2006.03.005

information is particularly important when non-linear behavior and permanent deformations occur. Most non-linear models whose parameters have physical or phenomenological interpretations are composed of non-linear functions of the deformation displacements and velocities. In order to identify those parameters which make up these non-linear functions of the displacements and velocities, one often needs to have access to those signals. Typically these are however not directly available, because accelerations are most commonly measured. Although it is common practice, for example in earthquake ground motion data releases, to integrate accelerations to obtain velocities and again to obtain displacements this practice is fraught with major pitfalls. This point is particularly true for causal integration schemes that would be required for continuous monitoring setups.

Recent years have delivered tremendous advances in sensor technologies for dynamic system monitoring, particularly for wireless applications which are promising for large civil structures. In addition, global positioning system (GPS) receivers and the corresponding data processing is permitting newly refined accuracy for high speed position information. With these hardware advances coupled with cost reductions, spatially dense heterogenous sensor arrays are envisioned for large civil structures. The potential then exists to exploit redundancy in sensor information. In this paper, the fusion of measured acceleration data with collocated displacement data will be investigated. Based on displacement and acceleration measurements, velocity and displacement are estimated with improved accuracy by using the Kalman filtering technique. In realistic scenarios the measurements of displacements and accelerations are often taken at different rates, therefore, a multi-rate Kalman filter and smoother is also developed in this paper to process such situations.

2. A review of the integration problem

The challenges of integrating acceleration to obtain estimates of the velocity and displacement can be seen in its simplest form from the following basic equations:

$$\dot{x} = \int \ddot{x}\,\mathrm{d}t + c_1, \tag{1}$$

$$x = \int \dot{x}\,\mathrm{d}t + c_1 t + c_2, \tag{2}$$

where c_1 and c_2 are constants of integration. Notice that c_1 is a spurious mean level in velocity and then becomes a linear function in the displacement. In theory these can be removed with mean removal and detrending, but in practice, as is explained below, spurious low-frequency error due to measurement noise still exists within the estimated signals. Also, mean removal and detrending assumes that these quantities are truly spurious, which would not be true in the case of actual permanent deformation occurring during the response.

2.1. Time domain integration

Following similar presentations in Hamming [1] and Worden [2], one may consider several possible common time domain integration techniques to evaluate their relative performance. For example the third-order corrector integration scheme is characterized by the following equation:

$$y_{n+1} = y_n + \frac{\Delta t}{12}(5\dot{y}_{n+1} + 8\dot{y}_n - \dot{y}_{n-1}). \tag{3}$$

For convenience, a sampling frequency of $\Delta t = 1$ s is assumed, and therefore the angular Nyquist frequency will be π radians. Letting $f_n = \dot{y}_n$, one can write the discrete transfer function, i.e. $y_n = G(z)f_n$, of the third-order corrector integration rule as

$$G(z) = \frac{(1/12)(5 + 8z^{-1} - z^{-2})}{(1 - z^{-1})}. \tag{4}$$

Again, repeating concepts in [1] and [2], one is ultimately interested in the accuracy of the integration scheme whose discrete transfer function was just derived. This can be quantified as the Fourier Transform of the

estimate divided by the Fourier Transform of the exact integrated quantity (if it is available). This is then the frequency domain transfer function between the estimate and the exact integrated signal. Denoting 'FT' as Fourier Transform this is transfer function is written as:

$$H_{\text{accuracy}}(\omega) = \frac{FT(\text{estimate of integrated signal})}{FT(\text{exact integrated signal})}. \tag{5}$$

Expressing $z = e^{i\omega}$ in order to convert the discrete time transfer function $G(z)$ into a frequency domain transfer function $H(\omega)$, yields

$$H(\omega) = \frac{(1/12)(5 + 8e^{-i\omega} - e^{-2i\omega})}{(1 - e^{-i\omega})} = \frac{4 + 2\cos\omega + 3i\sin\omega}{-6 + 6\cos\omega + 6i\sin\omega}. \tag{6}$$

If the measured signal is the general signal $f = e^{i\omega t}$, the true integral should be $y = e^{i\omega t}/(i\omega)$, and the estimated output from the filter would be $y_{\text{est}} = H(\omega)e^{i\omega t}$, then

$$H_{\text{accuracy}}(\omega) = \frac{4 + 2\cos\omega + 3i\sin\omega}{-6 + 6\cos\omega + 6i\sin\omega}\,(i\omega). \tag{7}$$

Similar accuracy transfer functions can be obtained for other common integration rules, and a comparison is shown in Fig. 1. From this figure, one would recommend the choice of a sampling frequency, such that your frequencies of interest are no greater than about 15% of the Nyquist frequency. One can also look at the phase angle distortion introduced by these filters. It can be shown that all filters perform perfectly (i.e. no phase distortion) in this regard except for the third-order corrector which has some increasing phase distortion near the Nyquist frequency.

2.2. Noise amplification through integration

The prior discussion of integration accuracy did not include the effects of noise in the original acceleration records. Some spurious noise η_k at each k time sample is unavoidable, either from resolution error (truncation) or from background electrical noise in the data acquisition circuitry. Therefore, it is important to understand what the effect of the integrators is on that extraneous noise:

$$\begin{aligned} y_{k_{\text{est}}} &= G(z)(f_k + \eta_k) \\ &= y_k + G(z)\eta_k. \end{aligned} \tag{8}$$

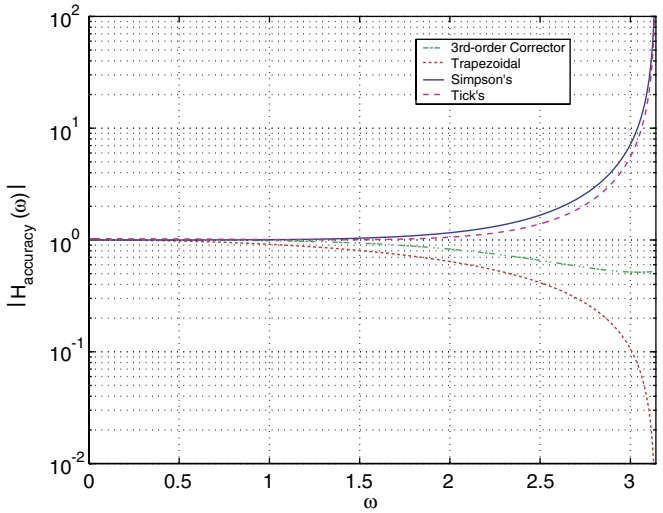

Fig. 1. A comparison of the magnitudes of the accuracy transfer function. The frequency axis is from zero to the Nyquist frequency. A value of unity would be optimal.

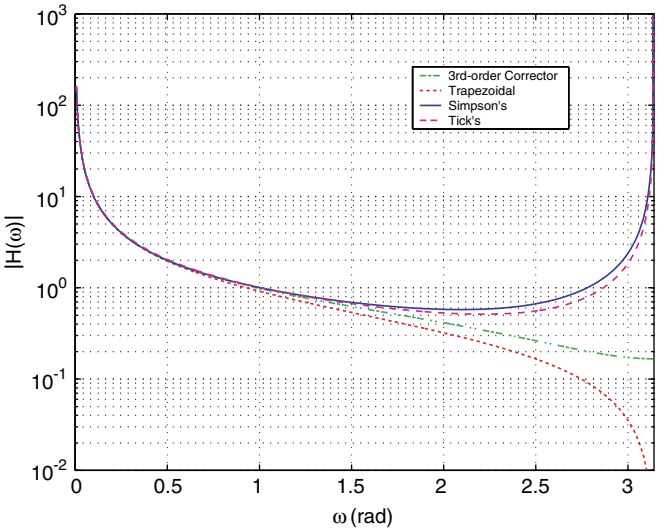

Fig. 2. Noise amplification magnitudes from one integration step. The smaller the amplification the better.

The error is therefore $\varepsilon_k = y_{k_{\text{est}}} - y_k = G(z)\eta_k$ and thus,

$$\frac{FT(\text{output noise})}{FT(\text{input noise})} = H(\omega). \tag{9}$$

This noise amplification is shown in Fig. 2 for each of the four integrators under consideration. This clearly shows what is an often experienced in reality; that low-frequency noise is greatly amplified through integration. In civil engineering applications, low-frequency spectral content is often critical, so any added and magnified disturbances in this frequency range can considerably complicate the data analysis, and system identification procedures. This also shows one of the key trade-offs, where previously it was concluded that one should stay below 15% Nyquist frequency if possible, this now seems to be one of the more problematic frequency ranges relative to the sampling rate, in that noise amplification is the greatest.

The effect of this noise amplification in many system identification approaches for non-linear system identification is the distortion of the observed states, i.e. the velocities and displacements, and the subsequent mis-identification of the associated model parameters.

2.3. Redundancy through displacement sensing

One reliable way of improving the accuracy of integration in the estimated displacement and velocity, is actually to augment the sensed motion to include displacement. This is not commonly done, and admittedly this could be quite expensive on a large scale, but the benefits are considerable. The most obvious of which is that one can track permanent deformation over time. Such permanent deformation is, of course, often associated with damage. This basic idea has been proposed for non-linear restoring-force mapping identification by Crawley and O'Donnell [3], where the measurement process itself was expressed in a state-space system formulation, and the observation error reduced through a simple error feedback approach from the control systems field. In this paper, an alternative and improved methodology using Kalman filtering for the accurate estimation for the displacement and velocity based on the dual acceleration and displacement measurement is explored.

3. Kalman filter formulation

Consider the case that acceleration and displacement are available to be measured. Then the measurement process can by modeled in state-space equation form as [3]

$$\begin{bmatrix} \dot{x} \\ \ddot{x} \end{bmatrix} = \begin{bmatrix} 0 & 1 \\ 0 & 0 \end{bmatrix} \begin{bmatrix} x \\ \dot{x} \end{bmatrix} + \begin{bmatrix} 0 \\ 1 \end{bmatrix} \ddot{x}_m + \begin{bmatrix} 0 \\ 1 \end{bmatrix} \eta_a, \tag{10}$$

$$z = x_m = [1\ \ 0]\begin{bmatrix} x \\ \dot{x} \end{bmatrix} + \eta_d, \tag{11}$$

where $\ddot{x}_m$ and x_m are the measured acceleration and displacement, η_a and η_d are the associated measurement noise of acceleration and displacement. It is assumed that η_a and η_d are white noise Gaussian processes with covariance q and r, respectively.

By introducing the state variables,

$$\mathbf{x} = \begin{bmatrix} x_1 \\ x_2 \end{bmatrix} = \begin{bmatrix} x \\ \dot{x} \end{bmatrix}. \tag{12}$$

Eqs. (10) and (11) can be compactly written in matrix form as

$$\dot{\mathbf{x}} = \mathbf{A}\mathbf{x} + \mathbf{B}u + \mathbf{w}, \tag{13}$$

$$z = \mathbf{H}\mathbf{x} + v, \tag{14}$$

where $\mathbf{w} \sim (0, \mathbf{Q})$, $\mathbf{Q} = \begin{bmatrix} 0 & 0 \\ 0 & q \end{bmatrix}$; $v \sim (0, \mathbf{R})$, $\mathbf{R} = r$. It is noted that Eqs. (13) and (14) rigorously represent the relationships between the states, the measurements and the associated measurement noises.

If acceleration is measured at the intervals of T_a, the system equation (10) and observation equation (11) can be discretized as

$$\begin{bmatrix} x_1(k+1) \\ x_2(k+1) \end{bmatrix} = \begin{bmatrix} 1 & T_a \\ 0 & 1 \end{bmatrix}\begin{bmatrix} x_1(k) \\ x_2(k) \end{bmatrix} + \begin{bmatrix} T_a^2/2 \\ T_a \end{bmatrix} u(k) + \begin{bmatrix} T_a^2/2 \\ T_a \end{bmatrix} \eta_a(k), \tag{15}$$

$$z(k) = [1\ \ 0]\begin{bmatrix} x_1(k) \\ x_2(k) \end{bmatrix} + \eta_d(k). \tag{16}$$

Written in compact form

$$\mathbf{x}(k+1) = \mathbf{A}_d\mathbf{x}(k) + \mathbf{B}_d u(k) + \mathbf{w}(k), \tag{17}$$

$$z(k) = \mathbf{H}\mathbf{x}(k) + v(k), \tag{18}$$

where $\mathbf{A}_d$ and $\mathbf{B}_d$ are derived by noting that $\mathbf{A}$ is nilpotent (i.e. $\mathbf{A}^2 = 0$)

$$\mathbf{A}_d = \mathrm{e}^{\mathbf{A}T_a} = \mathbf{I} + AT_a = \begin{bmatrix} 1 & T_a \\ 0 & 1 \end{bmatrix}, \tag{19}$$

$$\mathbf{B}_d = \int_0^{T_a} \mathrm{e}^{\mathbf{A}\tau}\mathbf{B}\,\mathrm{d}\tau = \mathbf{B}T_a + \frac{\mathbf{A}\mathbf{B}T_a^2}{2} = \begin{bmatrix} T_a^2/2 \\ T_a \end{bmatrix}. \tag{20}$$

The covariance matrices of the new discrete noise sequences can be obtained by [4]

$$\mathbf{Q}_d = \int_0^{T_a} \mathrm{e}^{\mathbf{A}\tau}\mathbf{Q}\mathrm{e}^{\mathbf{A}^{\mathrm{T}}\tau}\,\mathrm{d}\tau = \begin{bmatrix} qT_a^3/3 & qT_a^2/2 \\ qT_a^2/2 & qT_a \end{bmatrix}, \tag{21}$$

$$\mathbf{R}_d = \frac{\mathbf{R}}{T_a}. \tag{22}$$

The system equation (17) and observation equation (18) together make up the state-space representation of the formulation which a discrete-time Kalman filter can be applied in order to obtain accurate on-line estimates of the displacement and velocity. The Kalman filter algorithm for the above system can be summarized as

Time update:

$$\hat{\mathbf{x}}(k+1|k) = \mathbf{A}_d\hat{\mathbf{x}}(k|k) + \mathbf{B}_d u(k), \tag{23}$$

$$\mathbf{P}(k+1|k) = \mathbf{A}_d\mathbf{P}(k|k)\mathbf{A}_d^{\mathrm{T}} + \mathbf{Q}_d. \tag{24}$$

Measurement update:

$$\hat{\mathbf{x}}(k+1|k+1) = \hat{\mathbf{x}}(k+1|k) + \mathbf{K}(k+1)[z(k+1) - \mathbf{H}\hat{\mathbf{x}}(k+1|k)], \tag{25}$$

$$\mathbf{P}(k+1|k+1) = [\mathbf{I} - \mathbf{K}(k+1)\mathbf{H}]\mathbf{P}(k+1|k), \tag{26}$$

where Kalman gain $\mathbf{K}(k+1)$ is given by

$$\mathbf{K}(k+1) = \mathbf{P}(k+1|k)\mathbf{H}^{\mathrm{T}}[\mathbf{H}\mathbf{P}(k+1|k)\mathbf{H}^{\mathrm{T}} + \mathbf{R}_d]^{-1}. \tag{27}$$

4. Multi-rate Kalman filter

When the acceleration and displacement are measured at different sampling rates, a multi-rate Kalman filter can process the optimal estimates of the displacement and velocity. Assume the displacement measurement sampling interval is T_d, where $T_d/T_a = M$, M is an integer. Since no displacement measurements are available between the times kT_d, where k is an integer, this is equivalent to optimal filtering with arbitrarily large measurement errors [5], so $\mathbf{R}_d^{-1} \to 0$ and hence $\mathbf{K} \to 0$. Thus, only the time update is performed and the optimal estimate is

$$\hat{\mathbf{x}}(k+1|k+1) = \hat{\mathbf{x}}(k+1|k) = \mathbf{A}_d\hat{\mathbf{x}}(k|k) + \mathbf{B}_d u(k), \tag{28}$$

$$\mathbf{P}(k+1|k+1) = \mathbf{P}(k+1|k) = \mathbf{A}_d\mathbf{P}(k|k)\mathbf{A}_d^{\mathrm{T}} + \mathbf{Q}_d. \tag{29}$$

When displacement measurements are available at times kT_d, both the time update and measurement update should be performed. It is important to note that so far, as presented, this does not exploit the possible future 'correction' in displacement measurement as each displacement sample becomes available. Therefore, displacement estimates can drift within the large interval T_d. Thus some smoothing, albeit a non-causal procedure is beneficial.

5. Kalman filter smoothing

For on-line estimation, Kalman filtering provides the best estimates for the state of linear systems with additive Gaussian white noises. However, smoothing can produces a much better estimation by using measurements beyond the time of the states being estimated. The smoothing works through a combination of the forward Kalman filtering and backward filtering over the entire sequence of available measurements. Therefore, smoothing cannot be used in on-line data processing. In other words, the performance improvement is achieved at the expense of the on-line estimation. The Kalman filter smoothing can principally be classified into three categories, i.e. fixed-interval smoothing, fixed-point smoothing, and fixed-lag smoothing [6,7]. Fixed-interval smoothing estimates the sequence of state vectors at all sampling instants based on all measurements. Fixed-point smoothing permits one to use the entire sequence of measurements to estimate the state vector at a specific point. Fixed-lag smoothing is desirable when estimating the sequence of state vectors at a fixed time lag from the current observation process based upon all measurements. The smoothing algorithms investigated here are based on fixed-interval smoothing, however, the algorithms can also be used as fixed-lag smoothing estimators [8,9]. Brown and Hwang [10] proposed a simple way to implement fixed-lag smoothing by using Rauch–Tung–Striebel (RTS) algorithm [11] for fixed-interval smoothing in fixed-lag smoothing. This approach is accomplished by first filtering up to the current measurement and then sweeping back a fixed number of steps with the RTS algorithm. If the number of backward steps is small, then the state estimation is near 'on-line'. The number of backward steps $S = 5$ is used for all examples of smoothing in the later applications. The smoothed estimates $\hat{\mathbf{X}}(k|N)$ over $(0, N)$ can be obtained by

$$\hat{\mathbf{X}}(k|N) = \hat{\mathbf{X}}(k|k) + \mathbf{F}(k)[\hat{\mathbf{X}}(k+1|N) - \hat{\mathbf{X}}(k+1|k)], \tag{30}$$

where $\hat{\mathbf{X}}(k|k)$ is the updated state estimates from the forward multi-rate Kalman filter, and the smoothing gain $\mathbf{F}(k)$ is given by

$$\mathbf{F}(k) = \mathbf{P}(k|k)\mathbf{A}_d^{\mathrm{T}}\mathbf{P}^{-1}(k+1|k) \tag{31}$$

and $k = N-1, N-2, \ldots, 0$.

6. Applications

6.1. The swept-sine signal with an additional linear trend

Consider first an example of an analytically defined response signal: a swept-sine signal with an additional linear trend [12]. The time-history for the displacement can be expressed:

$$x(t) = \sin([a+\delta t]t) + bt. \tag{32}$$

Through direct differentiation one can obtain velocity and acceleration time-history

$$\dot{x}(t) = b + (a+2\delta t)\cos([a+\delta t]t), \tag{33}$$

$$\ddot{x}(t) = 2\delta\cos([a+\delta t]t) - (a+2\delta t)^2\sin([a+\delta t]t). \tag{34}$$

The first, and most important observation is, that the linear drift term is undetectable in the acceleration term. Therefore, no matter how accurate an acceleration sensor, it will not detect such a drift. Since the exact analytical time-histories of the displacement and velocity are known, it is possible to evaluate the performance of the proposed estimation scheme. In addition, the swept-sine signal is also a good signal to choose, because one can determine if methods are susceptible to changes in signal frequency content.

Here the acceleration sampling rate was chosen to be 1000 samples/s, i.e. the Nyquist frequency is 500 Hz. Such a high sampling rate is generally not required for most civil engineering applications, however it does offer some potential benefits for statistical methods which require a lot of averaged data, and also, it has the advantage that it can capture very high-frequency impact-like sudden response changes which might be associated with damage. (Such impact-like pulses were observed in the wind-shoe (deck-tower connection) area of the Vincent Thomas Bridge due to earthquake response during the 1994 Northridge earthquake [13]). For the multi-rate estimation case to be considered, the displacement measurement rate is 100 Hz, i.e. $M = 10$. A separate white noise process with 10% RMS noise-to-signal ratio is superimposed to both the exact analytical displacement and acceleration signals. These noise levels are reasonably realistic working environments for civil engineering applications.

Figs. 3 and 4 show the multi-rate Kalman filtering and Kalman filter smoothing results, respectively. To provide a sense of the shape and spectral content of the relative error, Figs. 5 and 6 show the multi-rate filtering errors and Kalman filter smoothing errors on a magnified scale. It can be seen that the schemes provide excellent estimates of both the velocity and the displacement including tracking of the drift term. In these multi-rate cases the RMS error is on the order of 2.5% for both signals. Note the RMS error for the single-rate case (i.e. when $M = 10$, and in this case both with a sample rate of 100 Hz) is also relatively low, in the range of 4–11% for the displacement and velocity, respectively, and in a similar comparison plot to Figs. 3 or 4, the estimated and exact signals would also appear nearly indistinguishable. This single-rate case is the worst case because in the multi-rate cases additional acceleration information is available. In all cases the linear trend is correctly identified in the displacement.

6.2. SDOF hysteretic system simulation

Here we consider a SDOF non-linear hysteretic Bouc–Wen system subject to recorded ground motion from the 1999 Chi–Chi earthquake.

$$m\ddot{x}(t) + c\dot{x}(t) + kr(t) = -m\ddot{x}_g(t), \tag{35}$$

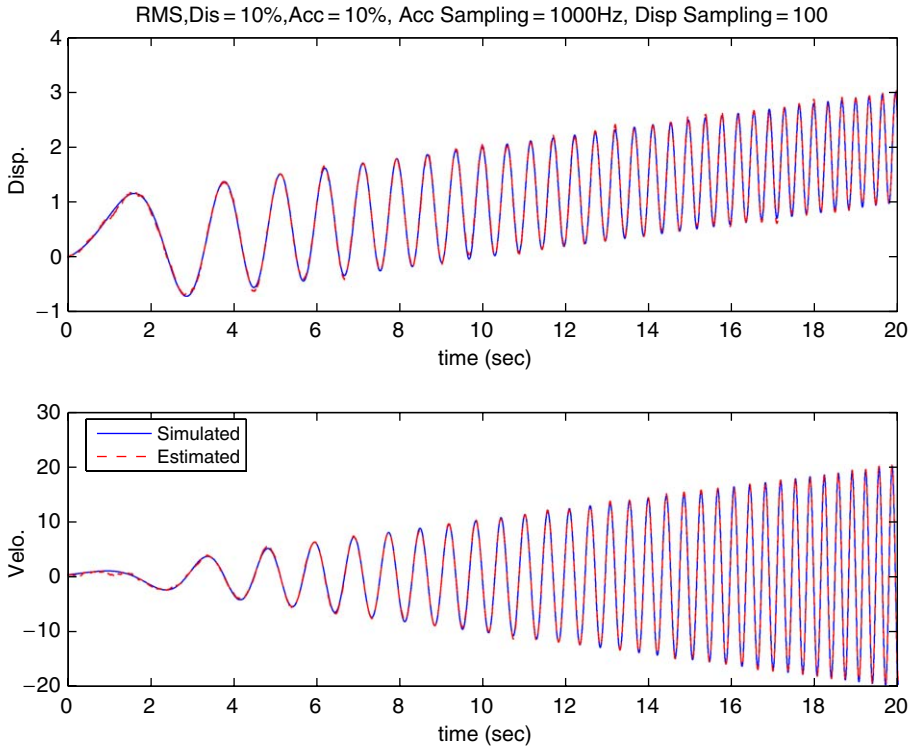

Fig. 3. Multi-rate Kalman filtering, $M = 10$.

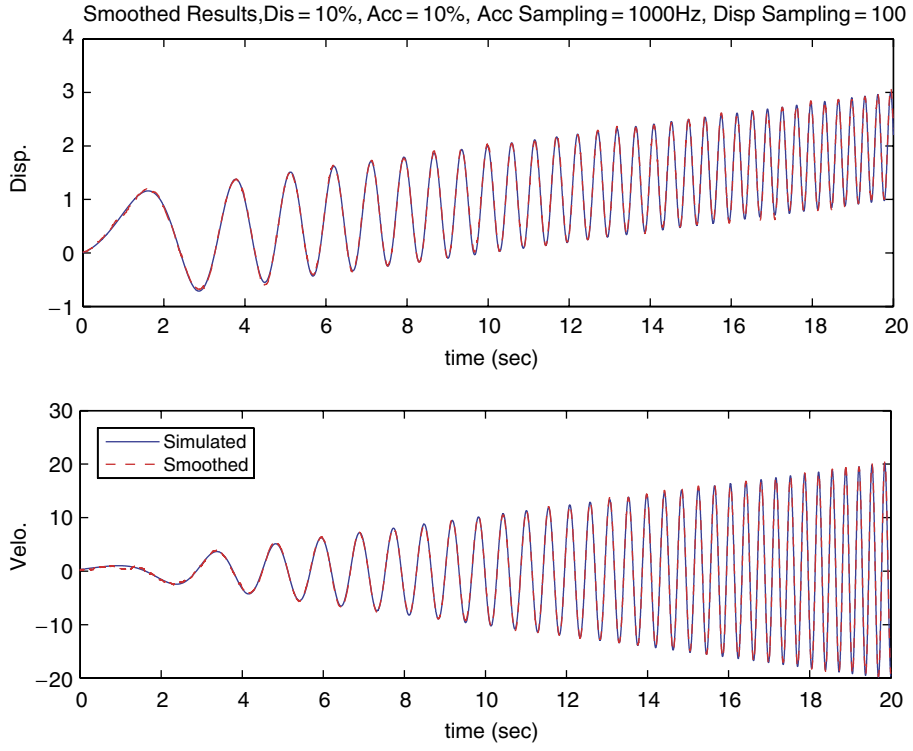

Fig. 4. Kalman filter smoothing, $S = 5$.

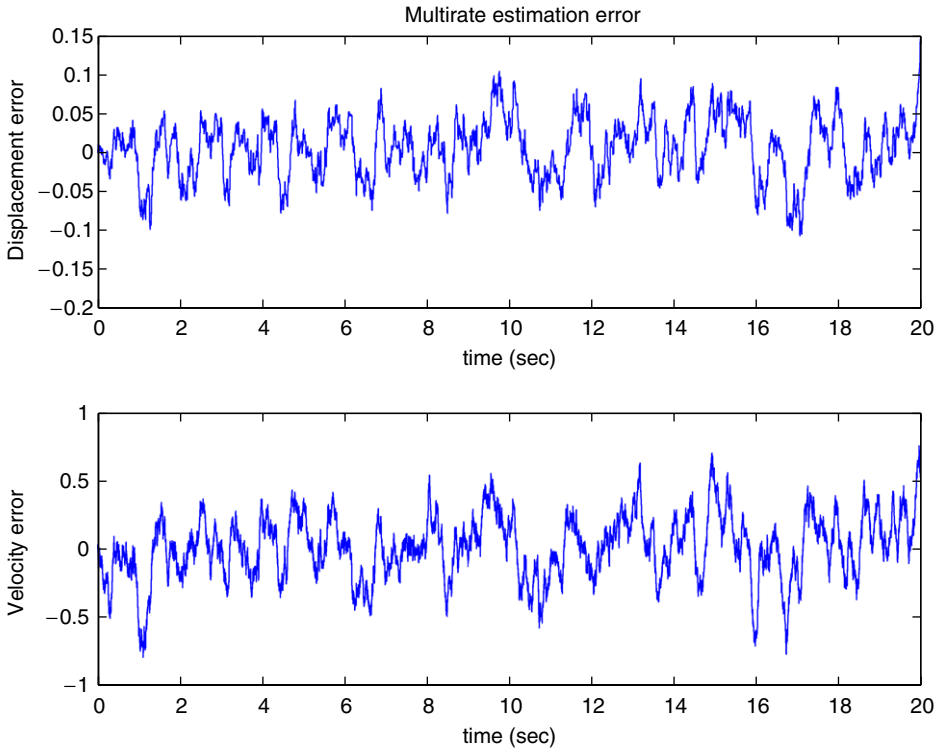

Fig. 5. Multi-rate estimation error of displacement and velocity.

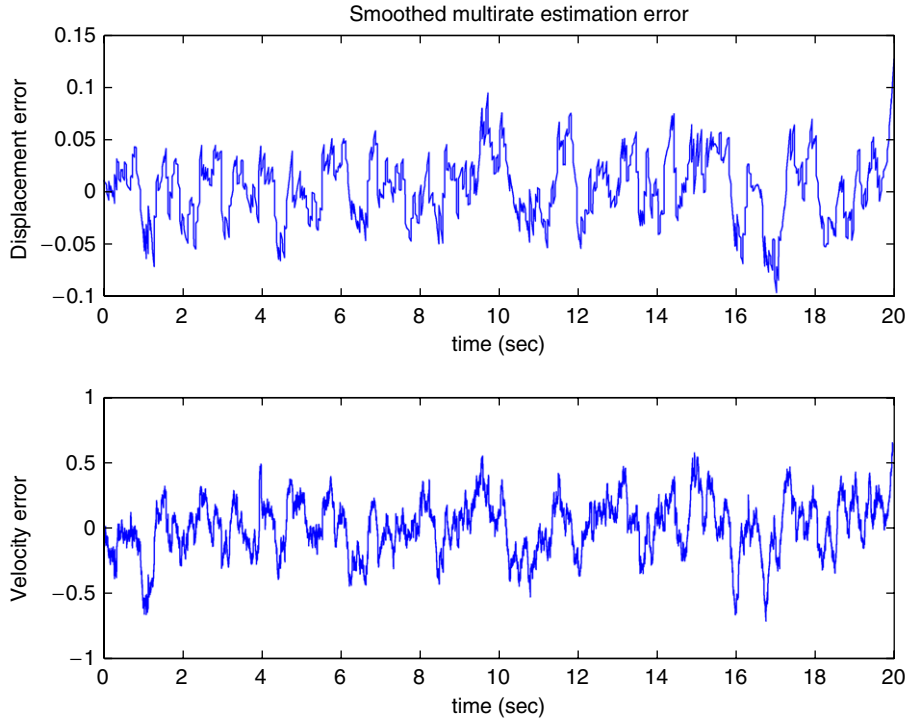

Fig. 6. Smoothed multi-rate estimation error of displacement and velocity.

where $r(t)$ is the Bouc–Wen hysteretic component with

$$\dot{r} = \dot{x} - \beta|\dot{x}||r|^{n-1}r - \gamma\dot{x}|r|^{n}. \tag{36}$$

Here $m = 1$, $c = 0.3$, $k = 9$, $\beta = 2$, $\gamma = 1$, $n = 2$. The sampling frequency of the recorded Chi–Chi earthquake acceleration is 250 Hz. The Chi–Chi earthquake signal was first filtered with a low-frequency cutoff of 0.03 Hz and the high-frequency cutoff of 50 Hz [14]. A duration of 40 s of the earthquake record was adopted in this example. The system responses of displacement and the acceleration were obtained by solving the ODE equation (35). The sampling frequency for the measurement of acceleration and displacement is 250 Hz. For the multi-rate estimation problem, the slower displacement sampling frequency is 25 Hz. A white noise process with 10% RMS noise-to-signal is superimposed to the simulated displacement and acceleration responses. Notice here that the displacement response has a drift component which would be very important to detect if one were interested in identifying a behavioral model, or simply for detecting permanent offset at the end of the response.

As in the previous case, the single rate Kalman filter estimates of velocity and displacement can be seen to be relatively accurate (with about 11% and 5% respective RMS error), and the corresponding plot is omitted here. Figs. 7 and 8 show the multi-rate Kalman filtering and smoothing results for the estimated velocity and displacement. Again, as can be seen, the proposed techniques estimate the velocity and displacement very well with on the order of 3.8% and 2.8% respective RMS error.

6.3. SDOF linear system simulation

In this example we consider the following SDOF linear system subject to same Chi–Chi earthquake acceleration excitation.

$$m\ddot{x}(t) + c\dot{x}(t) + kx = -m\ddot{x}_g(t), \tag{37}$$

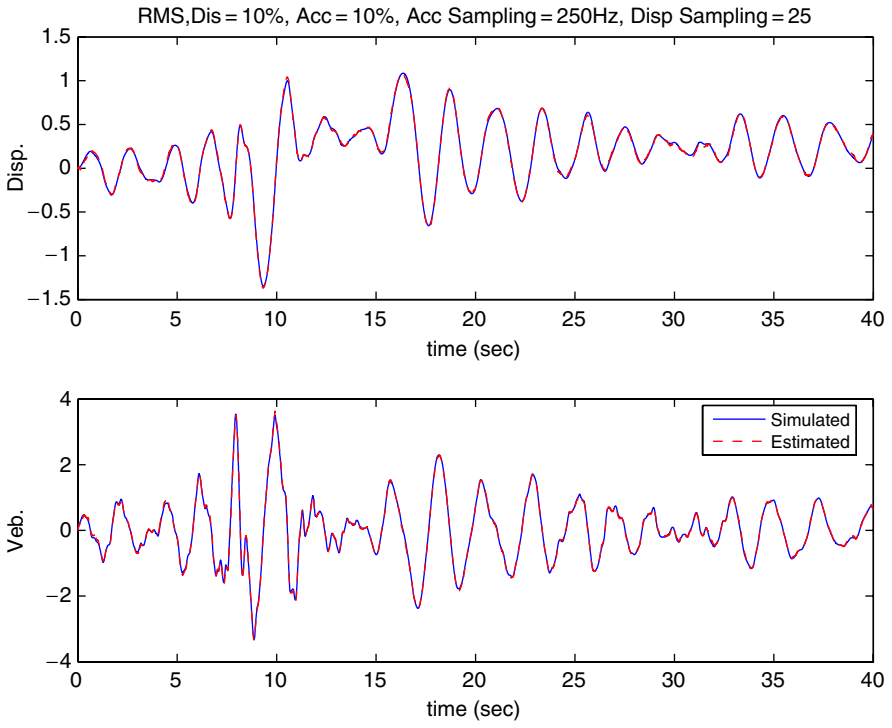

Fig. 7. The multi-rate Kalman filtering estimates of velocity and displacement response of a Bouc–Wen hysteretic element, with $M = 10$.

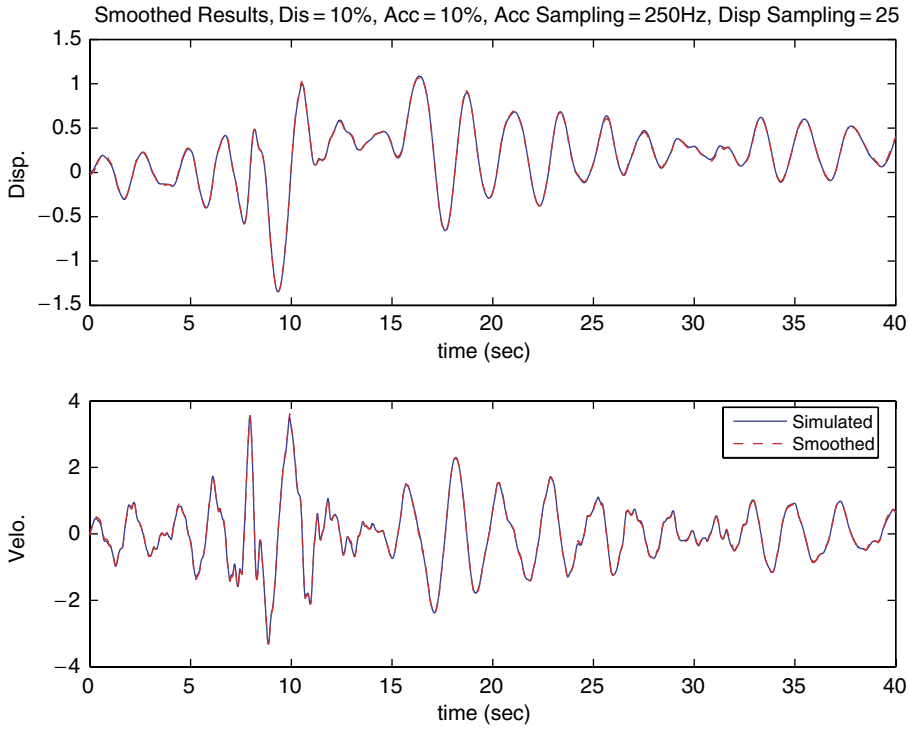

Fig. 8. The Kalman filter smoothing estimates of velocity and displacement response of a Bouc–Wen hysteretic element, with $M = 10$ and $S = 5$.

where $m = 1$, $c = 0.3$, $k = 9$. The excitation signal was the same in the hysteretic case. The sampling frequency of Chi–Chi earthquake acceleration is 250 Hz. First we use Newmark's method to solve the ODE equation (37) to obtain the system responses of displacement and the acceleration.

6.3.1. *Base case*

The measurement sampling frequency of acceleration and displacement is 250 Hz. For the multi-rate estimation problem, the slow displacement sampling frequency is 25 Hz. A white noise process with 10% RMS noise-to-signal ratio is superimposed to the simulated displacement and acceleration.

Both the single-rate and multi-rate Kalman filter estimates of velocity and displacement were determined. A sample of the multi-rate (without smoothing) performance is shown in Fig. 9. The estimation errors are shown in Fig. 10, and although not shown here, those for the smoothed case are of a similar order of magnitude, i.e. about 2.5% and 1.5% RMS levels of the displacement and velocity signals, respectively, but smoother.

6.3.2. *Effect of measurement noise level*

A 10% measurement noise level is considered to be within a normal working range for civil engineering applications. However, in order to evaluate the robustness of the proposed schemes to noise level, high noise level contaminated measurements of the acceleration and displacement were also considered.

In addition to the base case of 10% added noise, Table 1 provides a comparison of the RMS error obtained using the single-rate (25 Hz), multi-rate and multi-rate Kalman filter technique with smoothing for noise levels of 20% to 50%, respectively. It is observed from the table that the proposed techniques are very robust despite high levels of noise. Note that RMS noise levels of 50% are considered high for civil applications, and this would normally pose significant processing challenges.

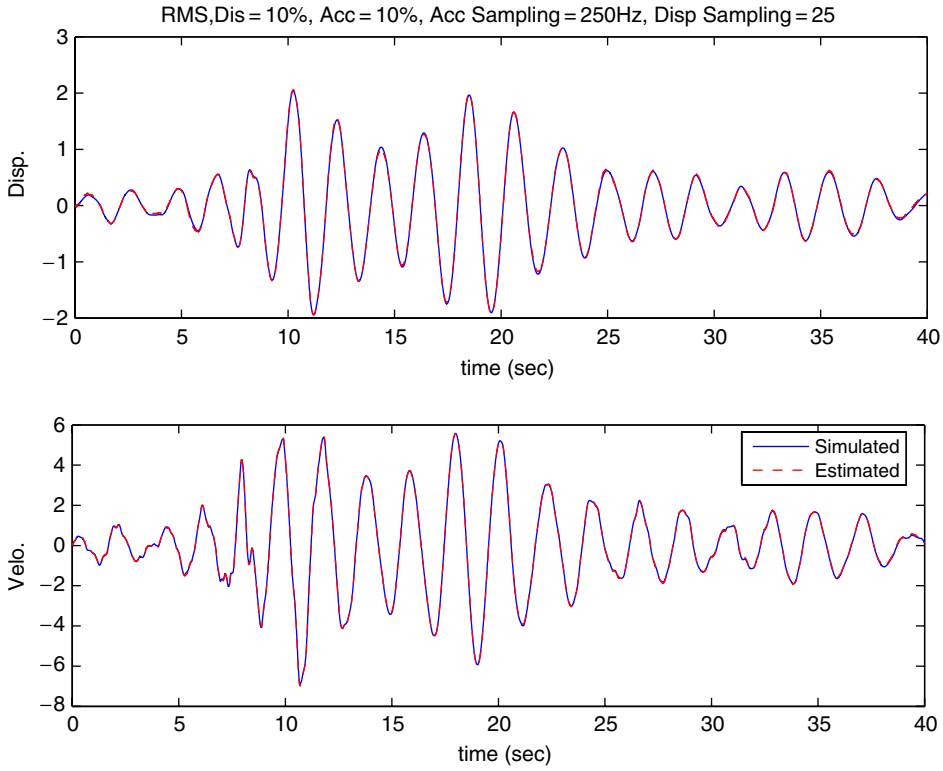

Fig. 9. Multi-rate Kalman filtering for linear SDOF system responses, $M = 10$.

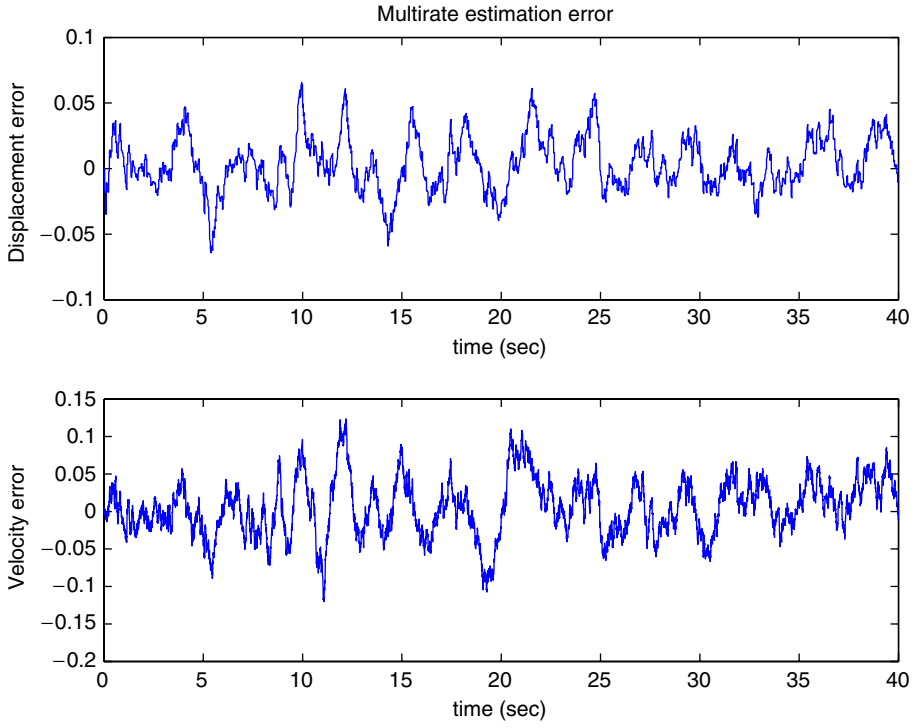

Fig. 10. Multi-rate estimation error of displacement and velocity.

Table 1
Normalized RMS error of estimates for different noise levels

Estimation	Noise level				
	10%	20%	30%	40%	50%
Single rate					
Displacement NRMS%	4.85	8.63	13.41	15.98	19.82
Velocity NRMS%	8.10	10.60	16.17	18.93	21.96
Multi-rate					
Displacement NRMS%	2.85	6.10	9.20	11.35	15.65
Velocity NRMS%	1.76	3.61	5.84	7.40	10.49
Smoothing					
Displacement NRMS%	2.32	4.80	6.97	8.52	12.11
Velocity NRMS%	1.58	3.11	5.01	6.43	9.25

For the multi-rate cases $M = 10$.

Table 2
Normalized RMS error of estimates for different displacement sampling rates

Estimation	M			
	10	20	50	100
Single rate				
Displacement NRMS%	4.85	8.73	13.86	17.87
Velocity NRMS%	8.10	17.09	38.02	73.60
Multi-rate				
Displacement NRMS%	2.85	3.82	6.30	6.43
Velocity NRMS%	1.76	2.24	2.42	2.74
Smoothing				
Displacement NRMS%	2.32	2.49	4.07	3.53
Velocity NRMS%	1.58	1.74	1.70	1.64

Note 'single rate' denotes the fact that both acceleration and displacement measurements are made at a slow rate, e.g. $M = 10$ implies here 25 Hz.

6.3.3. *Effect of displacement sampling rate*

It is common for the displacement measurement rate to be slower than the acceleration sampling rate. Also, if the displacement is measured by a GPS system, it is common that GPS measurements can be somewhat intermittent. In such a case, multi-rate Kalman filtering and smoothing will improve the estimation accuracy. In order to evaluate the capability of the proposed methods to deal with the multi-rate data processing problem, the displacement measurement is purposely made at a very slow rate. Here for the multi-rate cases considered the acceleration sampling rate is always 250 Hz, however, the displacement measurement rate is set to 12.5, 5 and 2.5 Hz, i.e. $M = 20$, 50 and 100, respectively. All the measurements of displacement and acceleration are simulated and white noise with a 10% RMS level is superimposed to model the measurement noise. A summary table of the normalized RMS errors of the estimated signals versus the exact signals is given in Table 2.

Fig. 11 shows the estimates of the velocity and displacement for one of the cases considered. Here both acceleration and displacement are measured at a single (slow) rate of 5 Hz. Despite this severe limitation the normalized RMS error as shown in Table 2 is on the order of 14% and 38% for the displacement and velocity, respectively. When the high rate (250 Hz) acceleration data is combined with the 5 Hz sampled displacement and one also uses the proposed smoothing step, one can see a drastic improvement in signal estimation in

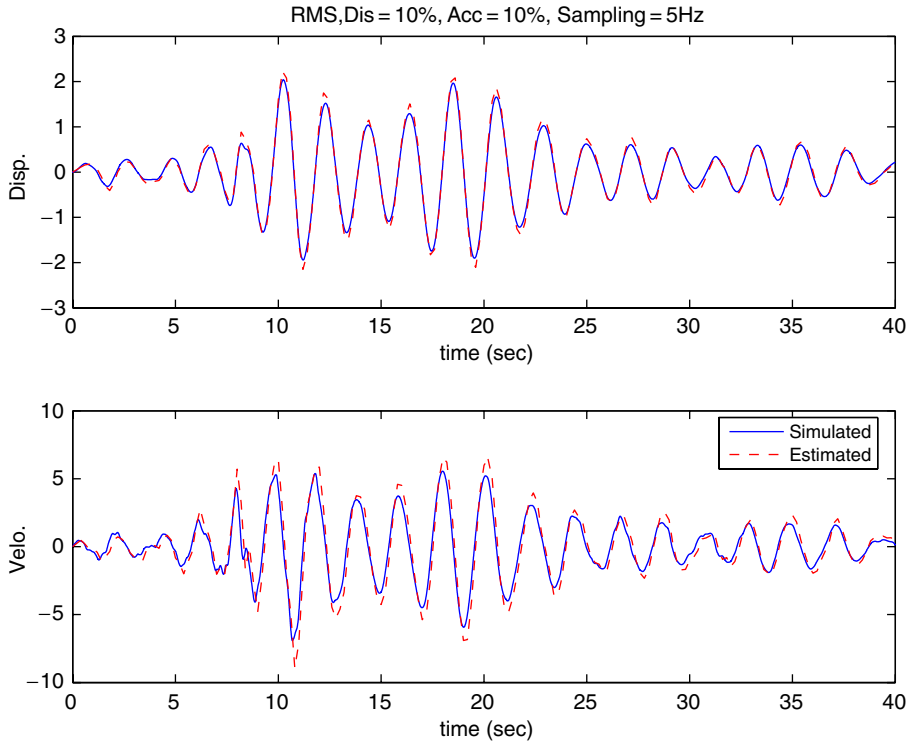

Fig. 11. Signal estimates from single (slow) rate Kalman filtering for linear SDOF system responses, both the acceleration and displacement sampling rate are 5 Hz.

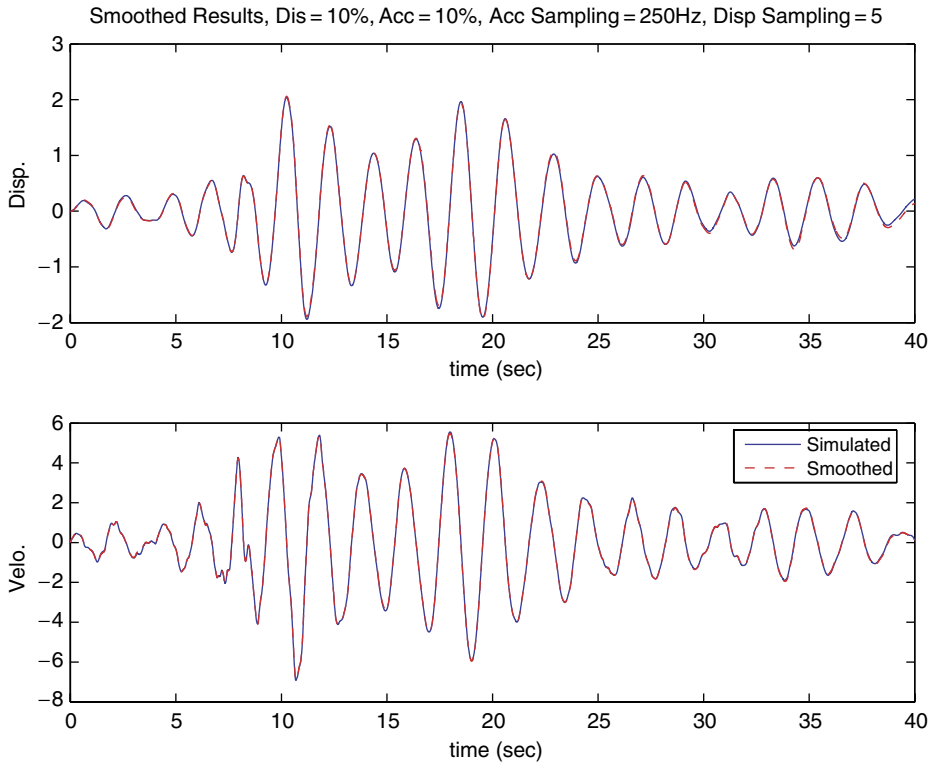

Fig. 12. Signal estimates from multi-rate Kalman filtering with smoothing, $M = 50$ and $S = 5$.

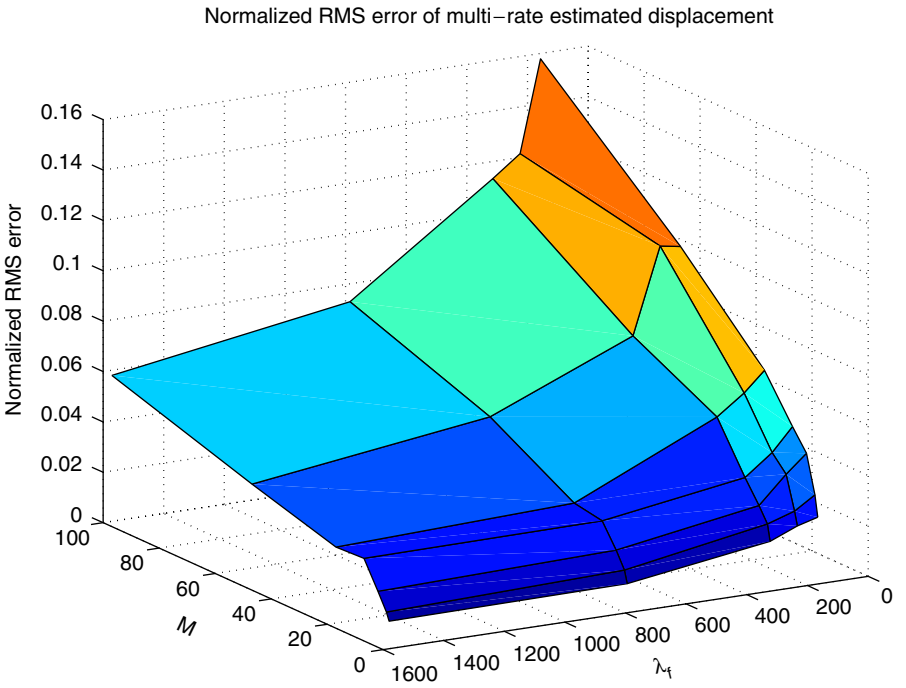

Fig. 13. Normalized displacement RMS error for multi-rate estimation.

Fig. 12, with normalized RMS error of about 1.7% and 4%, respectively. The estimated results demonstrate that the proposed techniques can track the velocity and displacement very well even for the very slow displacement measurement sample rates.

In order to appreciate the performance of the proposed approach in a general non-dimensionalized manner Figs. 13–16 show the normalized RMS error surfaces of the multi-rate Kalman filtering and with smoothing with respect to the variation of the displacement measurement rate f_d and system natural frequency f_N for this example. The acceleration measurement rate is fixed at 250 Hz. It can be seen that the proposed schemes are quite robust, providing relatively low RMS error even for extreme ratios of acceleration sampling rate f_a to displacement sampling rate f_d and ratios of the acceleration sampling rate to system natural frequency f_N. For example when $\lambda_f = f_a/f_N = 50\pi$ and $M = 100$ one still has only on the order of 7% and 3% RMS error in the velocity and displacement error, respectively, when the smoothing procedure is included.

6.4. Extension beyond low-sample rate Nyquist frequency in displacement

According to Nyquist–Shannon sampling theorem, the highest frequency that we can expect to be present in the sampled signal is the Nyquist frequency. The Nyquist frequency is the bandwidth of a sampled signal, and is equal to half the sampling frequency of that signal. As previously mentioned displacements are often measured at a relatively low sampling frequency. Under this scenario, it is possible that the signal frequency content that is higher than the Nyquist frequency and will be impossible to detect from the low sampling rate displacement measurement. This problem can be also benefit from the developed multi-rate filtering and smoothing technique.

Consider, for example, the following analytically defined non-stationary acceleration response signal:

$$\ddot{x}(t) = te^{at}[\sin(\omega_1 t) + b\sin(\omega_2 t)]. \tag{38}$$

Through direct integration one can obtain analytical solutions of velocity and displacement time-histories. Here the acceleration sampling rate was chosen to be 100 Hz, i.e. the Nyquist frequency is 50 Hz; and the displacement measurement rate is 5 Hz, i.e. the Nyquist frequency is 2.5 Hz and $M = 20$. ω_1 and ω_2 were

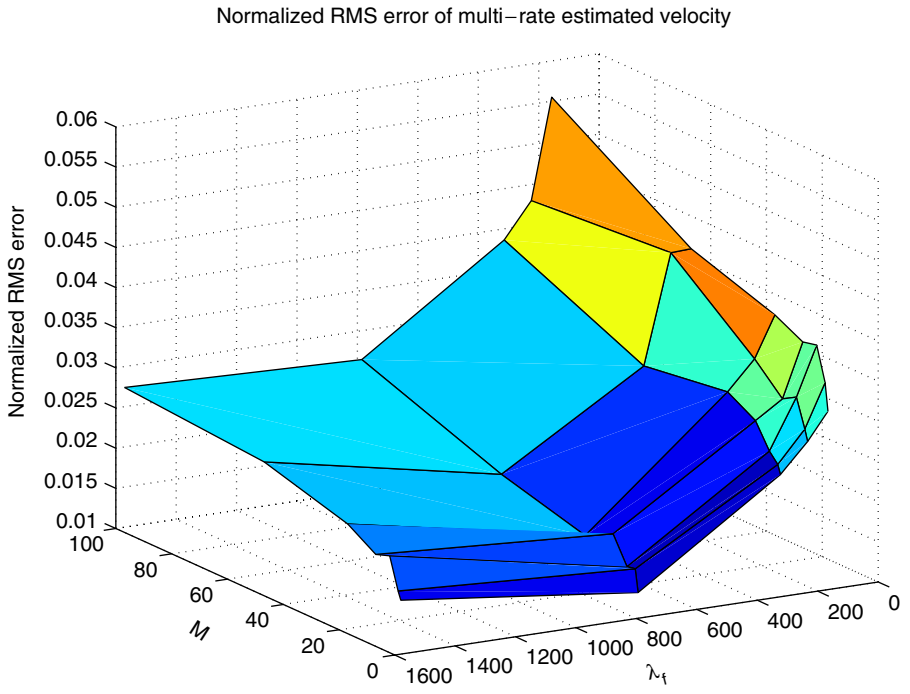

Fig. 14. Normalized velocity RMS error for multi-rate estimation.

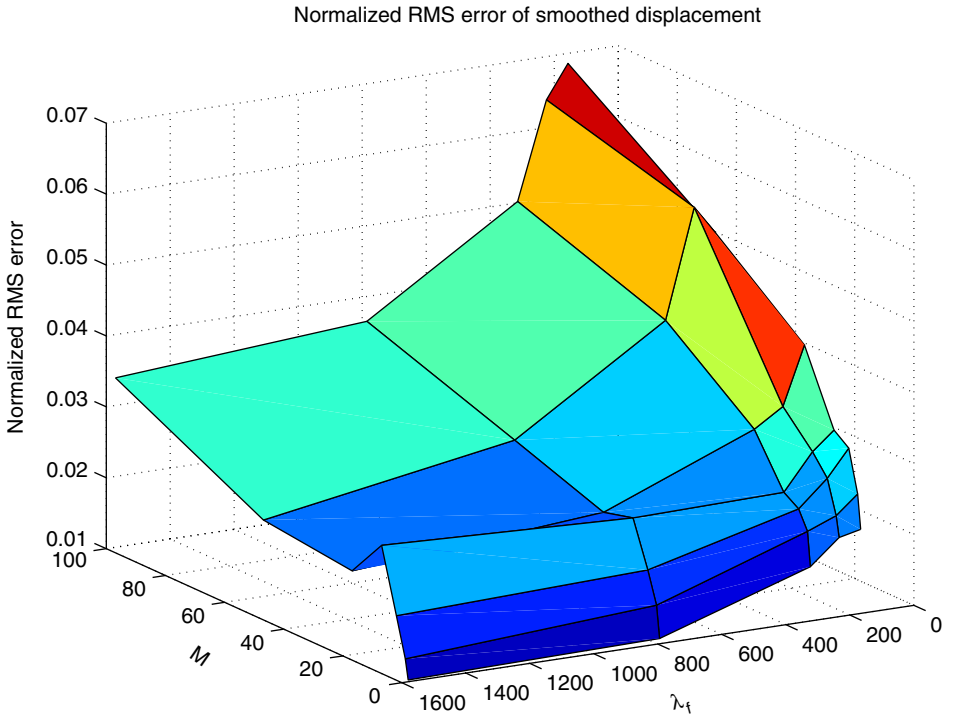

Fig. 15. Normalized displacement RMS error for smoothed multi-rate estimation.

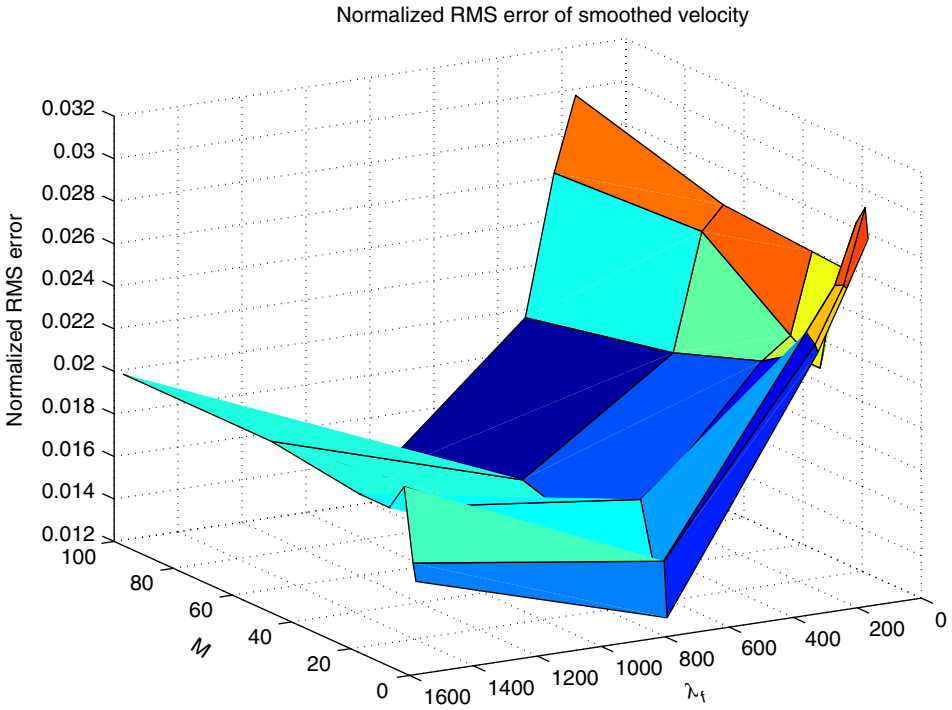

Fig. 16. Normalized velocity RMS error for smoothed multi-rate estimation.

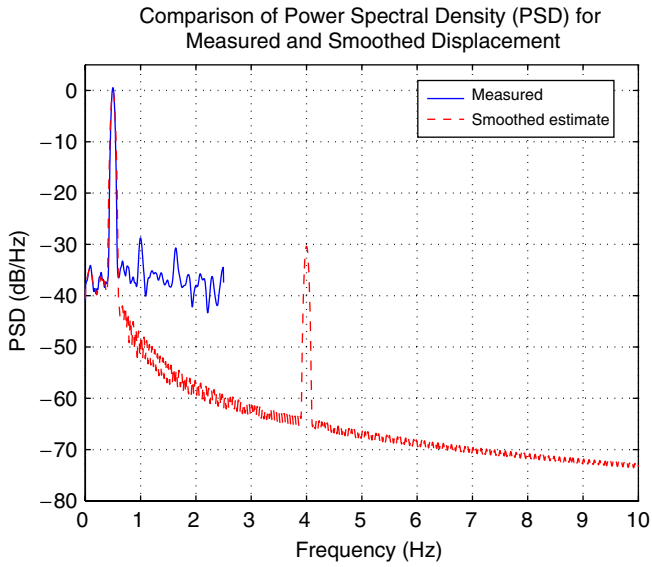

Fig. 17. Comparison of power spectral density (PSD) for measured and smoothed displacement.

chosen to be π and 8π so that the signal contains frequencies of 0.5 and 4 Hz, i.e. one is higher and the other is lower than the Nyquist frequency of the displacement measurement. The measurement noise level considered here is 10%. Through the developed multi-rate Kalman filtering and smoothing technique, the comparison of power spectral density (PSD) obtained using Welch's method for measured and smoothed displacement is shown in Fig. 17. It clearly shows that the frequency of 4 Hz which is higher than Nyquist frequency can be directly detected from the smoothed displacement, while, it is undetectable from the low sampling rate

displacement measurement. It is interesting to note, that in the PSD of the original noise-contaminated low sampled displacement the 4 Hz component aliases as a 1 Hz peak as expected. This aliasing problem is obviously also circumvented by producing the estimated high sample rate displacement.

7. Conclusions

A Kalman filtering and smoothing technique, which is capable of dealing with multi-rate estimates, has been investigated to accurately estimate the velocity and displacement from noise contaminated measurements of acceleration and displacement. The results show that the proposed schemes can estimate the velocity and displacement very accurately even with a high noise level and very slow displacement measurement. The multi-rate aspect permits a relatively low sampling rate for the displacement measurement which is shown to be sufficient to correct what might otherwise be low-frequency integration errors. In short it permits each sensor type to play to its inherent strengths; accelerometers will more easily detect higher frequencies, and low-frequency displacements can be detected by LVDT's, optical or GPS-based sensing which sometimes are limited to lower sampling rates.

Acknowledgements

This study was supported in part by the US National Science Foundation under CAREER grant CMS-0134333.

References

[1] R.W. Hamming, Digital Filters, 3rd ed., Prentice-Hall, Englewood Cliffs, NJ, 1989.
[2] K. Worden, Data processing and experiment design for the restoring force surface method, part I: integration and differentiation of measured time data, Mechanical System and Signal Processing 4 (4) (1990) 295–319.
[3] E.F. Crawley, K.J. O'Donnell, Force-state mapping identification of nonlinear joints, AIAA Journal 25 (7) (1987) 1003–1010.
[4] F.L. Lewis, Optimal Estimation: with an Introduction to Stochastic Control Theory, Wiley, New York, 1986.
[5] A. Gelb (Ed.), Applied Optimal Estimation, MIT Press, Cambridge, 1974.
[6] J.S. Meditch, Stochastic Optimal Linear Estimation and Control, McGraw-Hill, New York, 1969.
[7] T.F. Elbert, Estimation and Control of Systems, Van Nostrand Reinhold, New York, 1984.
[8] E.H. Shin, N. El-Sheimy, Optimizing smoothing computation for near real-time GPS measurement gap filling in INS/GPS systems, in: Proceedings of the US Institute of Navigation (ION) GPS 2002, Portland, 2002.
[9] C. Hide, T. Moore, Low cost sensors, high quality integration, in: Proceedings of NAV/AIS04, London, 2004.
[10] R.G. Brown, P.Y.C. Hwang, Introduction to Random Signals and Applied Kalman Filtering, third ed., Wiley, New York, 1997.
[11] H.E. Rauch, F. Tung, C.T. Striebel, Maximum likelihood estimates of linear dynamic systems, AIAA Journal 3 (8) (1965) 1445–1450.
[12] A. Smyth, Structural monitoring motion sensors: a user perspective, in: Caltrans/UCSD Workshop on Structural Health Monitoring and Diagnostics of Bridge Infrastructure, San Diego, 2003.
[13] A.W. Smyth, J.-S. Pei, S.F. Masri, System identification of the Vincent Thomas suspension bridge using earthquake records, Earthquake Engineering and Structural Dynamics 32 (3) (2003) 339–367.
[14] PEER strong motion database, ⟨http://peer.berkeley.edu/smcat/⟩, June 2005.